中國機械工程學刊第四十二卷第四期第 361~370 頁(民國一百一十年)
Journal of the Chinese Society of Mechanical Engineers, Vol.42, No.4, pp. 361~370 (2021)

A Study on Dynamic Analysis of Helical Geared Rotor System With Oil-Film Bearing

Ying-Chung Chen*, Wen-Cheng Lu**and Siu-Tong Choi***

Keywords：rotor dynamic, oil-film bearing, finite element, helical gear pair.

ABSTRACT

This study employs the finite element method to analyze the dynamic behavior of a helical geared rotor system with oil-film bearing. The system comprises the rotating shaft, helical gear pair, and oil-film bearing. The Timoshenko beam model is used to simulate the rotating shaft, and the rotating shaft's rotational inertia and shear strain effect are considered. In consideration of the gyroscopic effect, the helical gear pair is assumed to be two rigid disks, and a linear spring and damper are connected along the pressure line of the disks for simulation. This study investigates the effects of bearing lubricant viscosity, bearing radial clearance, bearing diameter, bearing length, bearing length-to-diameter ratio, helix angle, and an inner diameter of the rotating shaft on the systems' axial and lateral dynamic response for determining the system's dynamic properties. The simulation results serve as a reference for academic researchers and industrial practitioners wishing to further investigate helical gear rotor systems with oil-film bearings.

INTRODUCTION

Rotary dynamics play critical roles in various engineering fields. Rotating machines are commonly used in both large and small industrial equipment including aero engines, steam turbines, wind power generators, internal combustion engines, reciprocating compressors, and centrifugal compressors, all of which involve rotating shaft mechanisms. Therefore, discussion and research on rotating machines are crucial.

Gears are the primary power transfer component in rotating machines. Unsuitable gear selection or inadequate gear design may result in noise and vibration during gear meshing, thereby causing energy loss and damage to components. Spur gears are the most commonly employed type of gear in rotating systems. Although they are easy to manufacture and have low production costs, spur gears have a low gear occlusion rate during gear meshing and thus generate considerable vibration and noise. However, gears that vibrate excessively during gear meshing often sustain damage. To solve these problems in the operation of spur gear rotor-bearing systems, this study proposes the replacement of spur gears with helical gears. Helical gears have advantages in power transfer applications, including stable power transfer and high-speed operation. Therefore, using helical gears in rotating gear fields can effectively reduce the amount of vibration and noise that are generated. Furthermore, helical gears are viable for use in systems operating at high speed.

Bearings are the main component supporting rotors in rotating machines. Because of their simple structure, high load capacity, adequate stability, and long working life, oil-film bearings are commonly employed in rotating machines. Studies on rotor system bearings have generally employed linear bearings. However, the increased complexity of the current rotor-bearing systems has raised issues in rotating machine design, including how the problems with nonlinear systems can be simulated and analyzed using linear methods, how resonance can be prevented in rotor systems, and how system stability can be increased.

Ruhl and Booker (1972) used the finite element model to analyze a rotor-bearing system, in which the Euler–Bernoulli beam theory was used in the shaft model that took into account the bending moment and translational inertia of the shaft. Their numerical results showed that this method could be used to precisely analyze a rotor-bearing system. Nelson and McVaugh (1976) subsequently adopted the Rayleigh beam theory to simulate a rotating shaft, considering the rotatory inertia of the disk, the axial force, and the

Paper Received June, 2020. Revised December, 2021. Accepted January, 2021. Author for Correspondence:Ying-Chung Chen.

** Assistant Professor, Department of Aeronautical and Mechanical Engineering, Air Force Academy, Kaohsiung, Taiwan 820, ROC.*

*** Graduate Student, Department of Aeronautics and Astronautics, National Cheng Kung University, Tainan, Taiwan 701, ROC.*

**** Professor, Department of Aeronautics and Astronautics, National Cheng Kung University, Tainan, Taiwan 701, ROC.*

gyroscopic effect to obtain the system's equation of motion. They also derived the dynamic response and critical rotational speed of the rotor-bearing system. Nelson (1980) used the Timoshenko beam theory and the finite element model to calculate the effect of shear deformation and rotatory inertia and compared the values obtained with those using Euler beam (1973), and Rayleigh beam (1969). The results indicated that the Timoshenko beam was affected by shear deformation and rotatory inertia, and thus had a lower natural frequency than the Euler–Bernoulli, and Rayleigh beams.

To analyze the dynamic behavior of oil-film bearings, scholars have conducted experimental research to determine the effects of radial clearance, oil-film viscosity, and the rotation speed of the rotation shaft on the oil-film force or magnitude of vibration. Lund and Saibel (1967) expanded the two stiffness coefficients and two damping coefficients of the oil-film bearing into four stiffness coefficients and four damping coefficients, making the oil-film system model more accurate. Vance and Kirton (1975) explored that the dynamic pressure oil-film force which is from the incompressible lubricating fluid between the squeezed oil-film bearings, and the value is similar to the theoretical value derived from the Reynolds equation. Thomsen and Andersen (1974) studied the effect of oil-film viscosity and pointed out that for small amplitudes, the damping coefficient and the rotating speed of the shaft are independent of the vibration. Lin and Lin (2001) analyzed the stability of the rotor system with oil-film bearing and changed the size of the shaft to optimize the weight of the system.

About the study of helical geared rotor-bearing systems, Lund (1978) analyzed the dynamic response and critical speed of the system by considering the influence of gear eccentricity and transmission error. The results indicate that the influence of high-frequency system transmission error is negligible. Kahraman (1993) developed a helical geared rotor-bearing system for simulation and explored the dynamic effect of the helical angle, with results indicating that the natural frequency was not considerably affected by this angle. Kahraman (1994) also explored the effect of a helical geared rotor-bearing system's natural frequency and mode by changing the helical angle. Results show that gear meshing affected lateral, axial, and torsional mode coupling. Kubur (2004) extended the model into a three-axis two-pair geared-rotor system model. Draca (2006) discussed the natural frequency and response of the helical geared rotor-bearing system with the different positions of the disk and the length of the shaft. Feng et al. (2011) analyzed the influence of bearing stiffness coefficient on the dynamic response of the helical geared rotor-bearing system. Yang et al. (2012) developed a double-helical geared rotor-bearing system whose gear stiffness changed over time, with results indicating that the system produced higher dynamic responses in particular positions at several natural frequencies. Zhang et al. (2013) developed a general three-dimensional dynamic model of helical gear pairs with geometric eccentricity. The gear mesh and bearing flexibility is included in the model as well. Wang et al. (2018) developed an improved time-varying mesh stiffness (TVMS) model of a helical gear pair, in which the total mesh stiffness contains the axial tooth bending stiffness, axial tooth torsional stiffness, and axial gear foundation stiffness. Ali et al. (2019) developed six degrees of freedom dynamic model of a planetary geared rotor system which includes gyroscopic effects.

Although some dynamic factors have been incorporated into the dynamic analysis of the geared rotor-bearing system, few studies have considered the oil-film bearing in dynamic modeling. This study introduces a novel dynamic model for a helical geared rotor system with oil-film bearing, which investigates the effects of bearing lubricant viscosity, bearing radial clearance, bearing diameter, bearing length, bearing length-to-diameter ratio, helix angle, and an inner diameter of the rotating shaft on the systems' axial and lateral dynamic response for determining the system's dynamic properties.

DERIVING THE SYSTEM EQUATION OF MOTION

Figure 1 displays the helical geared rotor-bearing system discussed in this study. The system includes rotating shafts, oil-film bearings, and a helical gear pair. The rotating shaft is considered to be a flexible Timoshenko beam with a shear deformation effect and uses oil-film bearings as the system bearings. This paper used a fixed coordinate system (X, Y, Z) to describe the equation of motion. Figure 2 shows the typical rotor configuration and coordinates, U is the axial displacement along the X-axis, V and W indicate the system's lateral displacement along the Y and Z axes. B and Γ are rotational displacements along the Y and Z, respectively, α is the torsional displacement. The helical gear pair is viewed as two rigid disks. The helical gear pair is mounted on a rotating shaft and modeled as a linear spring and damper along its pressure line. First, the Lagrange equation and finite element model are used to construct the equations of motion of the system. Subsequently, the equations are combined through superposition to obtain the equation of motion of the complete system. This equation is analyzed to reveal the system's dynamic properties.

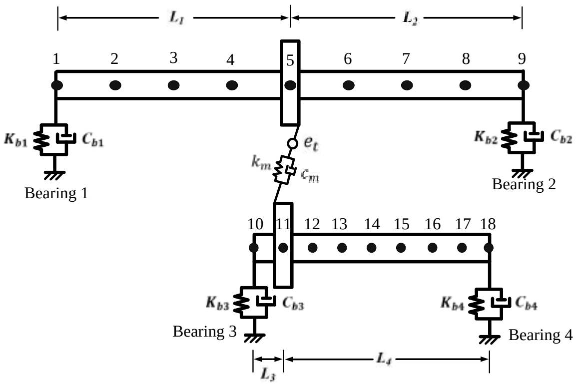

Fig. 1. A model of the helical geared rotor-bearing system.

Disk and Gear Mesh

Each gear has six degrees of freedom: one degree of axial displacement U_d, two degrees of lateral displacement V_d and W_d, and three degrees of rotational displacement α_d, B_d and Γ_d. Because this study considers the gears to be rigid, the effect of strain energy is ignored. The kinetic energy equations of the gears are as follows:

$$\begin{aligned}T_{\mathrm{D}} &= \frac{1}{2}m[(\dot{U}_d)^2+(\dot{V}_d)^2+(\dot{W}_d)^2]+\frac{1}{2}I_{dD}[(\dot{B}_d)^2+(\dot{\Gamma}_d)^2] \\ &+\frac{1}{2}I_{dP}[(\Omega+\dot{\alpha}_d)(\dot{B}_d\Gamma_d-\dot{\Gamma}_d B_d)+(\Omega+\dot{\alpha}_d)^2]+\frac{1}{2}me_d^2(\Omega+\dot{\alpha}_d)^2 \\ &+me_d(\Omega+\dot{\alpha}_d)[-\dot{V}_d\sin(\Omega t+\alpha_d+\Psi_d)+\dot{W}_d\cos(\Omega t+\alpha_d+\Psi_d)],\end{aligned} \tag{1}$$

where m is the gear mass; I_{dD} and I_{dP} are the mass and polar moment of inertia of the gear, respectively; Ω is the rotation speed of the rotating shaft; e_d is the eccentric distance of the gear, and Ψ_d is the phase angle of the gear. By inputting the kinetic energy equation (1) into the Lagrange equation, the kinetic energy equation of the gear is obtained:

$$[M_d]\{\ddot{q}_d\}+\Omega[G_d]\{\dot{q}_d\}=\{F_d\}, \tag{2}$$

where, $[M_d]$, $[G_d]$, $\{F_d\}$, and $\{q_d\}$ are the mass matrix, gyroscopic effect matrix, external force term, and displacement vector of the gear, respectively.

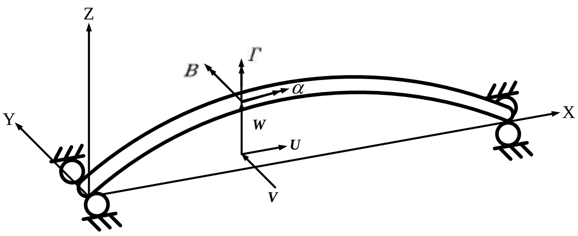

Fig. 2. Typical rotor configuration and coordinates (2020).

Figure 3 displays the helical gear pair model. The helical gear pair is mounted on a rotating shaft and modeled as a linear spring and damper along its pressure line. The gearmesh stiffness coefficient, k_m, is assumed to be a constant. The gearmesh damping coefficient c_m and transmission error e_t are ignored. The gearmesh force is calculated as follows:

$$F_h = k_m\delta. \tag{3}$$

The relative gear meshing displacement along the pressure line is determined as follows:

$$\begin{aligned}\delta &= [(V_{d2}-V_{d1})\sin\phi_p+(W_{d2}-W_{d1})\cos\phi_p-(r_{d1}\alpha_{d1}+r_{d2}\alpha_{d2})]\cos\phi_h \\ &+[(U_{d2}-U_{d1})+(r_{d1}B_{d1}+r_{d2}B_{d2})\sin\phi_p-(r_{d1}\Gamma_{d1}+r_{d2}\Gamma_{d2})\cos\phi_p]\sin\phi_h,\end{aligned} \tag{4}$$

where subscripts d_1, d_2 represent the driving and driven gears. r_{d1}, r_{d2}, ϕ_p, and ϕ_h are the driving gear radius, driven gear radius, pressure angle, and helix angle, respectively. From equations (2) and (3), the equation of motion of the gear pair is derived as follows (2013):

$$\begin{bmatrix}[M_{g1}] & 0 \\ 0 & [M_{g2}]\end{bmatrix}\{\ddot{q}_g\}+\Omega\begin{bmatrix}[G_{g1}] & 0 \\ 0 & \dfrac{N_{t1}}{N_{t2}}[G_{g2}]\end{bmatrix}\{\dot{q}_g\}+k_m[S_h]\{q_g\}=\{F_d\}, \tag{5}$$

where $[M_{g1}]$ and $[M_{g2}]$ are the mass matrix of the driving and driven gears, respectively; Ω is the rotating speed of the driving shaft; N_{t1} and N_{t2} are the number of teeth on the driving and driven gears, respectively; $[G_{g1}]$ and $[G_{g2}]$ are the gyroscopic effect matrix of the driving and driven gears, respectively; $[S_h]$ is the gearmesh stiffness matrix of the helical gear pair; $\{F_d\}$ is the eccentric force vector of the gear, and $\{q_g\}$ is the displacement vector of the helical gear pair.

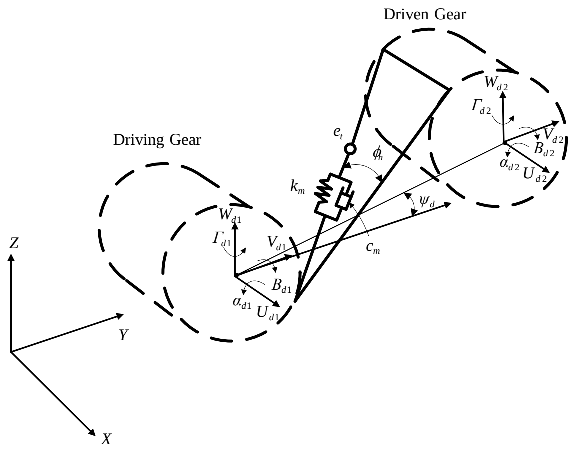

Fig. 3. A model of the helical gear pair.

Shaft

This study used the Timoshenko beam theory in developing the model. The effect of shear deformation and rotational inertia were considered and uses the finite element model to derive the equation of motion of the system. Figure 4 indicates that each rotating shaft element is composed of two nodes. Each node has six degrees of freedom, namely one degree of axial displacement U_s, two degrees of lateral displacement V_s and W_s, and three degrees of rotational displacement α_s, B_s and Γ_s. Therefore, each rotating shaft element has 12 degrees of freedom. The kinetic energy of the rotating shaft element is calculated as

$$T_s = \frac{1}{2}\int_0^l \left\{ \begin{array}{l} \rho A[(\dot{U}_s)^2 + (\dot{V}_s)^2 + (\dot{W}_s)^2)] + \rho I_{sD}[(\dot{\mathrm{B}}_s)^2 + (\dot{\Gamma}_s)^2] \\ +\rho I_{sP}(\Omega + \dot{\alpha}_s)(\dot{\mathrm{B}}_s \Gamma_s - \dot{\Gamma}_s \mathrm{B}_s) + \rho I_{sP}(\Omega + \dot{\alpha}_s)^2 \end{array} \right\} ds, \tag{6}$$

where ρ, A, I_{sD}, and I_{sP} are the density, cross-sectional area, moment of inertia, and polar moment of inertia of the shaft, respectively. The strain energy of the shaft element is calculated as follows:

$$\begin{aligned} U_s &= \frac{1}{2}\int_0^l \rho E I_{sD}[(\mathrm{B}_s')^2 + (\Gamma_s')^2]ds + \frac{1}{2}\int_0^l \rho G I_{sP}(\alpha_s')^2 ds \\ &+ \frac{1}{2}\int_0^l \kappa G A[(V_s' - \Gamma_s)^2 + (W_s' + \mathrm{B}_s)^2]ds + \frac{1}{2}\int_0^l EA(U_s')^2 ds, \end{aligned} \tag{7}$$

where E and G are Young's modulus and shear modulus of the shaft, respectively, and κ is the shear factor. By inputting the kinetic energy equation (6) and strain energy equation (7) into the Lagrange equation, the equation of motion of the shaft element is obtained as follows (2013):

$$[M_s]\{\ddot{q}_s\} + \Omega[G_s]\{\dot{q}_s\} + [K_s]\{q_s\} = \{0\}, \tag{8}$$

where $[M_s]$, $[G_s]$, and $[K_s]$ are the mass, gyroscopic effect, and stiffness matrixes of the shaft element, respectively.

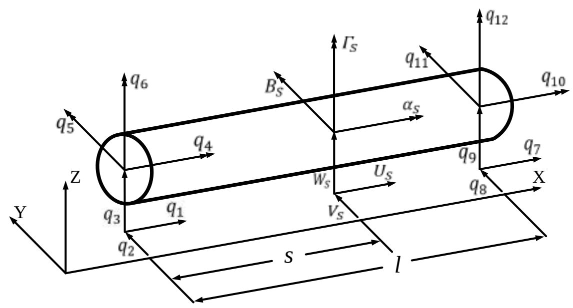

Fig. 4. Shaft element and the node degrees of freedom (2020).

Bearing

This study uses an oil-film bearing, which has low friction and heat generation. The motion conditions of the oil-film bearing are displayed in figure 5, with C, e, and W representing the radial clearance, eccentric distance, and radial load, respectively.

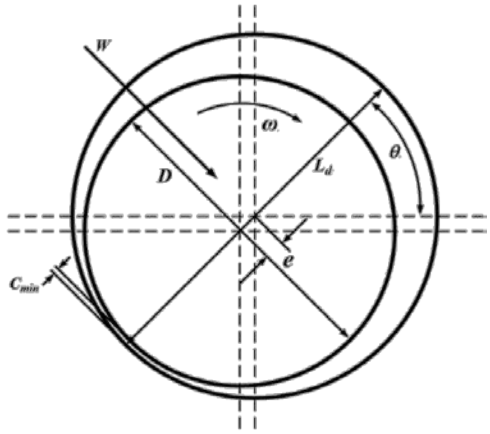

Fig. 5. A dynamic model of the oil-film bearing (2020).

This research hypothesizes that once the rotating shaft has achieved stable motion within the bearing, the stiffness and damping coefficients of the bearing are displayed as follows (2001):

$$\begin{aligned} k_{yy} &= \frac{4W\left\{\pi^2 + \left(32+\pi^2\right)\varepsilon^2 + 2\left(16-\pi^2\right)\varepsilon^4\right\}Q(\varepsilon)}{C\left(1-\varepsilon^2\right)}, \\ k_{yz} &= \frac{\pi W\left\{\pi^2 + \left(32+\pi^2\right)\varepsilon^2 + 2\left(16-\pi^2\right)\varepsilon^4\right\}Q(\varepsilon)}{C\varepsilon\sqrt{\left(1-\varepsilon^2\right)}}, \\ k_{zy} &= \frac{-\pi W\left\{\pi^2 - 2\pi^2\varepsilon^2 - \left(16-\pi^2\right)\varepsilon^4\right\}Q(\varepsilon)}{C\varepsilon\sqrt{\left(1-\varepsilon^2\right)}}, \\ k_{zz} &= \frac{4W\left\{2\pi^2 + \left(16-\pi^2\right)\varepsilon^2\right\}Q(\varepsilon)}{C}, \end{aligned} \tag{9}$$

$$\begin{aligned} c_{yy} &= \frac{2\pi W\left\{\pi^2 + 2\left(24-\pi^2\right)\varepsilon^2 + \pi^2\varepsilon^4\right\}Q(\varepsilon)}{\Omega C\varepsilon\sqrt{\left(1-\varepsilon^2\right)}}, \\ c_{yz} = c_{zy} &= \frac{8W\left\{\pi^2 + 2\left(\pi^2-8\right)\varepsilon^2\right\}Q(\varepsilon)}{\Omega C}, \\ c_{zz} &= \frac{2\pi W\sqrt{\left(1-\varepsilon^2\right)}\left\{\pi^2 + 2\left(\pi^2-8\right)\varepsilon^2\right\}Q(\varepsilon)}{\Omega C\varepsilon}, \end{aligned} \tag{10}$$

$$Q(\varepsilon) = [\pi^2(1\text{-}\varepsilon^2) + 16\varepsilon^2]^{-3/2}, \tag{11}$$

$$\varepsilon = \frac{e}{C}, \tag{12}$$

where ε is the eccentricity ratio of the bearing, which is computed using the bearing characteristic coefficient S_s as follows:

$$S_s = \frac{\mu\Omega}{W}\left[\frac{R}{C}\right]^2 \frac{L_d^3}{D} = \frac{(1\text{-}\varepsilon^2)^2}{\pi\varepsilon\sqrt{\pi^2(1\text{-}\varepsilon^2)+16\varepsilon^2}}, \qquad (13)$$

where L_d is the bearing length, μ is the bearing lubricant viscosity, Ω is the rotating speed of the shaft, R is the radius of the bearing, and D is the diameter of the bearing. Because this study employs a cylindrical bearing, D = 2R. The equation of motion of the bearing is as follows:

$$[C_b]\{\dot{q}_b\}+[K_b]\{q_b\}=\{0\}, \qquad (14)$$

where, $[C_b]$, $[K_b]$, and $\{q_b\}$ are the damping matrix, stiffness, and displacement vector of the bearing, respectively.

System Equation of Motion

The equations of motion of the system disk, gear meshing, shaft, and bearing unit were introduced in the above. The equations for each unit can be combined to produce the equation of motion of the entire helical geared rotor-bearing system, as follows:

$$[M]\{\ddot{q}\}+(\Omega\ [G]+[C])\{\dot{q}\}+[K]\{q\}=\{F\} \qquad (15)$$

where $[M]$, $[G]$, $[C]$, $[K]$, $\{F\}$, and $\{q\}$ represent the system mass matrix, gyroscopic effect matrix, damping matrix, stiffness matrix, force vector, and displacement vector, respectively.

RESULTS AND DISCUSSION

To verify the accuracy of the proposed model, we chose Kahraman's helical gear pair system (1993). In the helix gear pair system shown in figure 6, the gear ratio is 1, the face width is 0.03m, and the gear mesh coefficient is 2×10^8 N/m. The other material parameters are shown in table 1. As can be seen from figure 7, the natural frequencies obtained from the proposed model are similar to the results of Kahraman (1993), indicating that the proposed model has good accuracy.

The following data were used in the calculation for the helical geared rotor system with oil-film bearing. The shaft outer diameter is 0.05 m, the bearing axial stiffness is 1×10^9 N/m, the gearmesh stiffness is 1×10^8 N/m. The other parameter values of the system are given in Table 2.

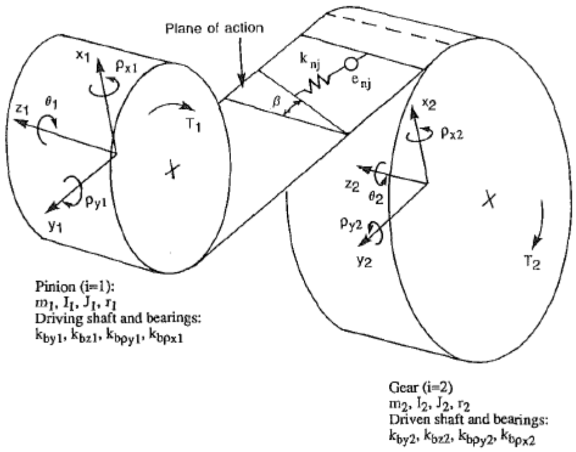

Fig. 6. Dynamic model of a helical gear pair system (1993).

Table 1. Helical gear pair parameters (1993).

Parameters	Pinion	Gear
Base circle radius (m)	0.05	0.05
Mass (kg)	2	2
I_i/r_{di}^2 (kg)	0.58	0.58
J_i/r_{di}^2 (kg)	1.16	1.16
k_{byi} (N/m)	3.5□10^8	3.5□10^8
k_{bzi} (N/m)	1□10^8	1□10^8
$k_{b\rho yi}/r_i^2$ (N/m)	1.1□10^8	1.1□10^8
Pressure angle (degrees)	20	
Transmission error (m)	1□10^{-6}	

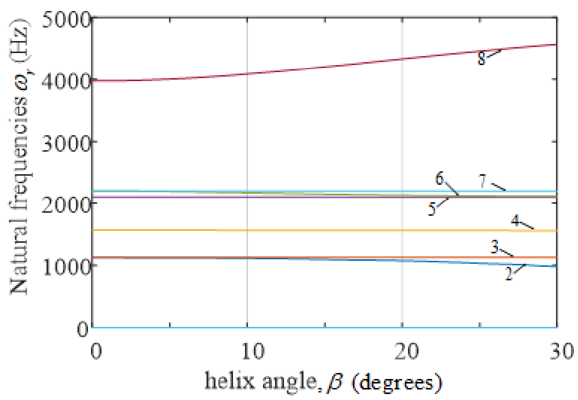

(a)

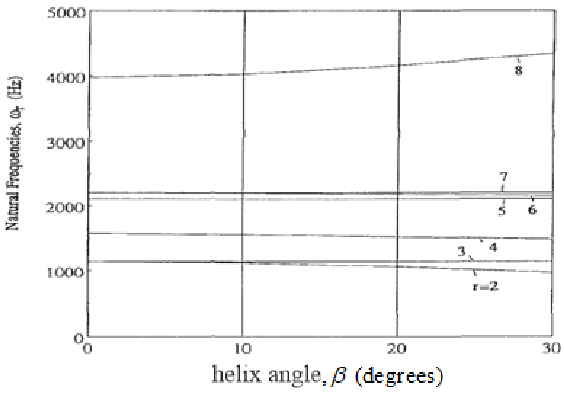

(b)

Fig. 7. Natural frequencies for the (a) proposed and (b) Kahraman (1993).

Table 2. Parameters of a helical geared rotor system with oil-film bearing.

Shaft parameters	
Shaft length (m)	$L_1 = 0.80,\ L_2 = 0.80,$ $L_3 = 0.10,\ L_4 = 0.70$
Density (kg/m^3)	7800
Young's modulus E (N/m^2)	2.07×10^{11}
Poisson's ratio v	0.3
Gear pair parameters	
Gear outer diameter (m)	0.30
Thickness (m)	0.03
Disk eccentricity (m)	$e_{d1} = e_{d2} = 1\times10^{-6}$
The phase angle of the gear (degree)	$\Psi_{d1} = \Psi_{d2} = 0$
Pressure angle (degree)	$\phi_p = 20$
Helix angle (degree)	$\phi_h = 20$
Bearing parameters	
Type of lubricant	SAE 40
Operating temperature (°C)	75
Radial clearance C (m)	5.00×10^{-6}
Bearing diameter (m)	0.08
Bearing length (m)	0.08

Effect of Bearing Lubricant Viscosity

This section discusses the influence of lubricant viscosity on the axial and lateral dynamic response of the rotor-bearing system. Lubricants with viscosity of 0.005, 0.01, 0.02, 0.05, 0.1, and 0.2 Pa·s are considered. The waterfall plot in figure 8 shows the lateral and axial dynamic response of the driving disk in the rotor-bearing system. Fig.8 reveals that the lateral and axial responses collectively decrease when the lubricant viscosity is increased. This is because, under the same rotation speed, the bearing viscosity and damping coefficients are higher when the lubricant viscosity is higher. Consequently, the lateral and axial dynamic response of the rotor-bearing system decrease when the lubricant viscosity is increased.

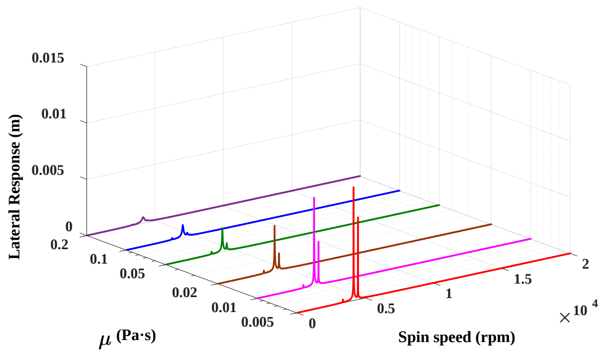

(a) lateral response ($\sqrt{V_{d1}^2 + W_{d1}^2}$)

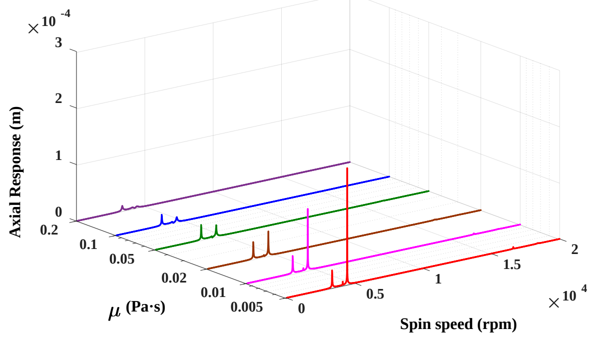

(b) axial response (U_{d1})

Fig. 8. Dynamic response of the driving disk under different lubricant viscosity.

Effect of Bearing Radial Clearance

This study hypothesizes that the lubricant flow is only laminar flow inside the radial clearance rather than turbulent or vortex flow. Therefore, the momentum effect within the lubricant flow is not computed. The following radial clearances (C) are considered: 2×10^{-6}, 4×10^{-6}, 6×10^{-6}, 8×10^{-6}, and 1×10^{-5} m. The waterfall plot presented in figure 9 shows the influence of radial clearance on the lateral and axial dynamic response of the driving disk. When the rotation speed of the rotor-bearing system is increased, the journal applies the lubricant to the radial clearance between the journal and the bearing. According to the incompressibility of liquid and hydrodynamic theory, the lubricant inside the radial clearance generates oil-film force. The oil-film has greater pressure if the radial clearance is small, thereby exerting a stronger influence on the system's dynamic response.

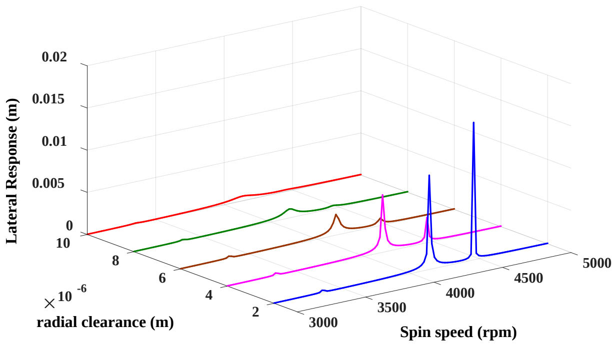

(a) lateral response ($\sqrt{V_{d1}^2 + W_{d1}^2}$)

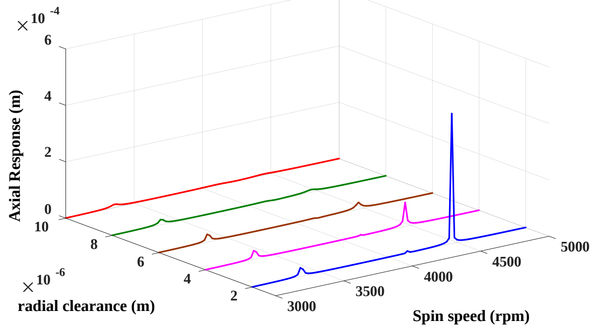

(b) axial response (U_{d1})

Fig. 9. Dynamic response of the driving disk under different radial clearance.

Effect of Bearing Diameter and Length

First, rotor-bearing systems with different bearing diameters (D) are employed to determine the influence of bearing diameters on the system's lateral and axial dynamic response. Rotor-bearing systems with bearing diameters of 0.06, 0.08, and 0.1 m are analyzed. Figure 10 displays the lateral and axial dynamic response of the driving disk in the rotor-bearing systems with different bearing diameters. The bearing diameter has a minimal influence on the system dynamic response. Subsequently, rotor-bearing systems with different bearing lengths (L_d) are used to determine the influence of the system, with the bearing lengths used being 0.06, 0.08, and 0.10 m. Figure 11 displays the lateral and axial dynamic response, and similar to the conclusion made from fig.10, fig. 11 reveals that bearing length has a minimal effect on the system's lateral and axial dynamic response. Finally, the influence of the length-to-diameter ratio (L_d/D) on the lateral and axial dynamic response is analyzed. Length-to-diameter ratios of 0.5, 1.0, 1.5, and 2.0 are considered. Figure 12 illustrates the lateral and axial dynamic response of the driving disk and indicates that when the length-to-diameter ratio is increased, the system stiffness and damping coefficients increase, whereas the lateral and axial dynamic response of the driving disk decreases. Besides, the system resonant frequency is higher when the length-to-diameter ratio is higher.

This case reveals that individually, bearing length and diameter do not notably influence the system's lateral and axial dynamic response. However, the length-to-diameter ratio does considerably affect the system's dynamic response.

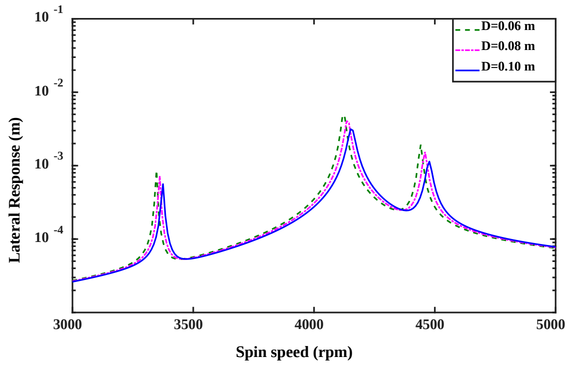

(a) lateral response ($\sqrt{V_{d1}^2 + W_{d1}^2}$)

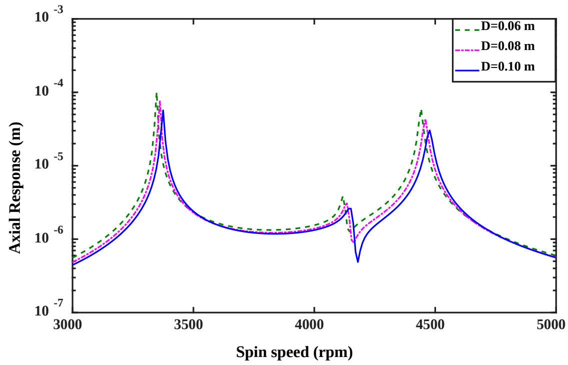

(b) axial response (U_{d1})

Fig. 10. Dynamic response of the driving disk under different bearing diameter.

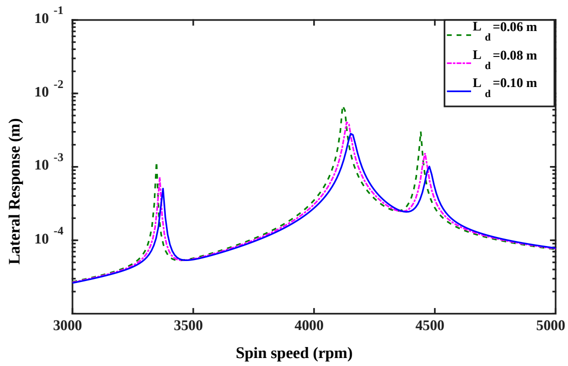

(a) lateral response ($\sqrt{V_{d1}^2 + W_{d1}^2}$)

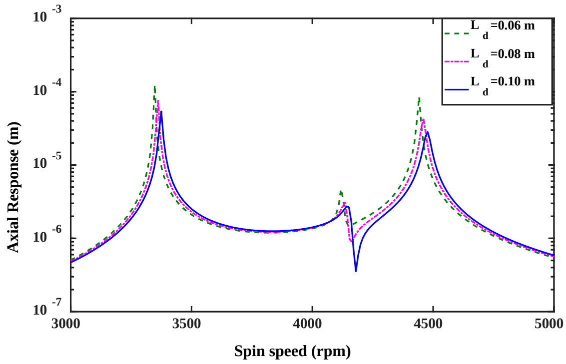

(b) axial response (U_{d1})

Fig. 11. Dynamic response of the driving disk under different bearing length.

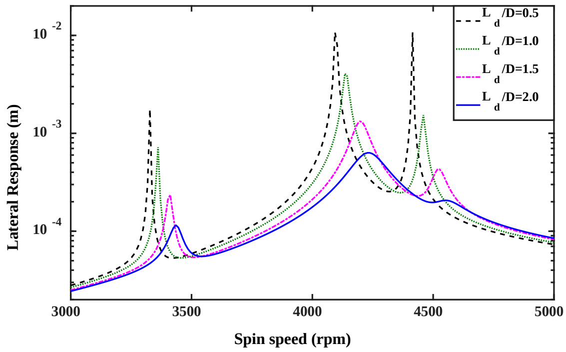

(a) lateral response ($\sqrt{V_{d1}^2+W_{d1}^2}$)

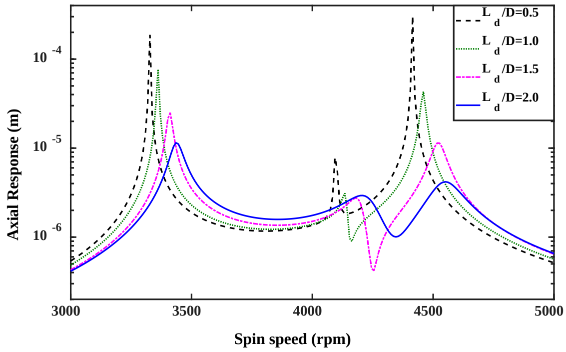

(b) axial response (U_{d1})

Fig. 12. Dynamic response of the driving disk under different length-to-diameter ratio.

Effect of Helix Angle

Current industrial applications of helical gears commonly adopt angles of 15° to 30°. This study compares the influence of different helix angles, namely 15°, 20°, and 25°, on the system's lateral and axial dynamic responses (figure 13). Greater degrees of helix angle indicates that more force is exerted in the axial direction and lesser force is invested into the lateral direction. When the helix angle was increased, the lateral and axial dynamic responses of the driving disk was decreased and increased, respectively.

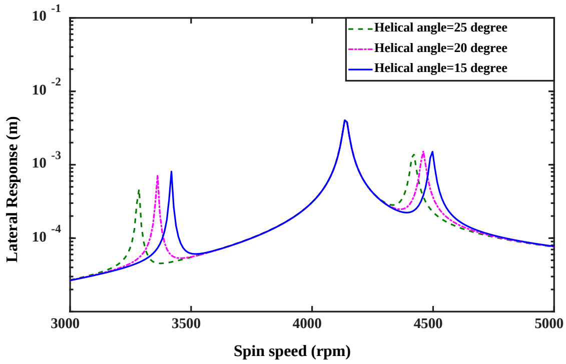

(a) lateral response ($\sqrt{V_{d1}^2+W_{d1}^2}$)

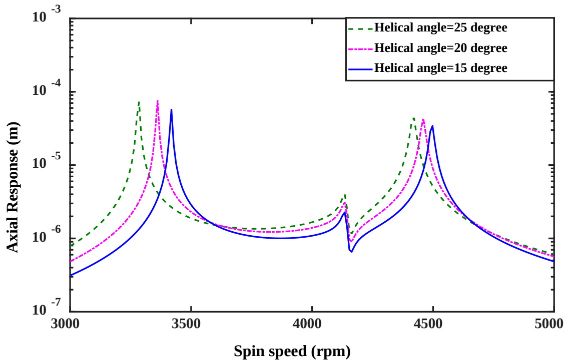

(b) axial response (U_{d1})

Fig. 13. Dynamic response of the driving disk under different helix angles.

Effect of Shaft Inside Diameter

Figure 14 displays the system's axial and lateral dynamic response when the inside diameter of the rotating shaft is 0.00, 0.02, and 0.04 m. A greater inside diameter results in a lower system stiffness coefficient and greater lateral and axial dynamic response of the driving disk. Similarly, the rotating shaft mass is lower when the inside diameter is greater. Although both the rotating shaft stiffness and mass decrease as the inside diameter is increased, under the parameters in this study, the rotating shaft mass significantly affects the system's natural frequency. Therefore, the system's natural frequency is higher when the inside diameter is greater.

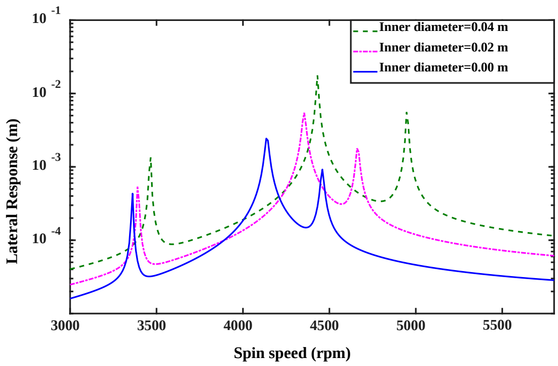

(a) lateral response ($\sqrt{V_{d1}^2+W_{d1}^2}$)

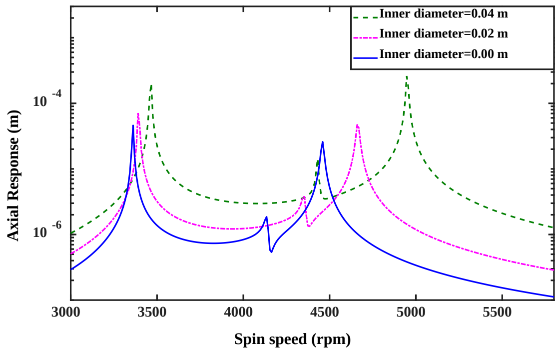

(b) axial response (U_{d1})

Fig. 14. Dynamic response of the driving disk under different shaft inside diameter.

CONCLUSIONS

Based on rotor dynamics, this study employs the finite element model to analyze the dynamic properties of helical geared rotor systems with oil-film bearings. To discuss the axial force of the helical gear, this study states that each node has six degrees of freedom. The effects of bearing lubricant viscosity, bearing radial clearance, bearing diameter, bearing length, bearing length-to-diameter ratio, helix angle, and inside diameter of the rotating shaft on the system's lateral and axial dynamic response are determined to analyze the system's dynamic properties. The numerical simulation results of this study reveal the following:

(1) The stiffness and damping coefficients of the bearing are higher when the lubricant viscosity is greater, resulting in a smaller lateral and axial dynamic response of the system.

(2) A smaller bearing radial clearance results in a greater oil-film force, thereby have greater pressure on the system's dynamic response.

(3) Individually, bearing length and diameter do not notably affect the system's lateral and axial dynamic response. However, the length-to-diameter ratio does considerably influence this response. The bearing stiffness and damping coefficients are higher when the length-to-diameter radio is higher, causing the system's lateral and axial dynamic response to be smaller. Besides, the system resonant frequency is higher when the length-to-diameter ratio is higher.

(4) When the helix angle is increased, the system's lateral response is decreased but the system's axial response is increased.

(5) An increase in the inside diameter of the rotating shaft causes the rotating shaft's stiffness and mass to decrease and causes the system's lateral and axial dynamic response to increasing. However, under the parameters of this study, the rotating shaft mass considerably influences the system's natural frequency. Therefore, the system's natural frequency is higher when the inside diameter of the rotating shaft is greater.

ACKNOWLEDGEMENTS

This research work was supported by the Ministry of Science and Technology of Taiwan (Grant No. 1072218E013001MY2).

REFERENCES

Ali, T., Christoph, W. S., Michael, I. F., "Dynamic behavior of three-dimensional planetary geared rotor system," *Mechanism and Machine Theory*, Vol. 134, pp. 39-56 (2019).

Chen, Y. C., Yang, T. H., Choi, S. T., "Dynamic analysis of a double-helical geared rotor system with oil-film bearing," *Aircraft Engineering and Aerospace Technology*, Vol. 92(4), pp. 653-662 (2020).

Dym, C. L., Shames, I. H., Solid Mechanics–A Variational Approach, McGraw-Hill, New York, (1973).

Draca, S., "Finite Element Model of a Double-Stage Helical Gear Reduction," M. S. Thesis, Department of Mechanical Engineering, University of Windsor, Canada (2006).

Eshleman, R. L., and Eubanks, R. A., "On the Critical Speeds of a Continuous Rotor," *Journal of Engineering for Industry ASME*, Vol. 91, pp. 1180-1188 (1969).

Feng, K., Matsumura, S., and Houjoh, H., "Dynamic Behavior of Helical Gears with Effects of Shaft and Bearing Flexibilities," *Applied Mechanics and Materials*, Vol. 86, pp. 26-29, (2011).

Kahraman, A., "Effect of Axial Vibration on the Dynamics of a Helical Gear Pair," *Journal of Vibration and Acoustics ASME*, Vol. 115, pp. 33-39 (1993).

Kahraman, A., "Dynamic Analysis of a Multi-Mesh Helical Gear Train," *Journal of Mechanical Design ASME*, Vol. 116, pp. 706-712 (1994).

Kubur, M., Kahraman, A., Zini, D. M., and Kienzle, K., "Dynamic Analysis of a Multi-Shaft Helical Gear Transmission by Finite Elements: Model and Experiments," *Journal of Mechanical Design ASME*, Vol. 126, pp. 398-406 (2004).

Lund, J. W., and Saibel, E., "Oil Whirl Orbits of a Rotor in Sleeve Bearing," *Journal of Engineering for Industry ASME*, Vol. 89, pp. 813-823 (1967).

Lund J., "Critical speed, stability and response of a geared train of rotors," *Journal of Mechanical Design ASME*, Vol. 100, pp. 535-539 (1978).

Lin, Y. H., and Lin, S. C., "Optimal Weight Design of Rotor Systems with Oil-Film Bearings Subjected to Frequency Constraints," *Finite Elements in Analysis and Design*, Vol. 37, pp. 777-798 (2001).

Nelson, H. D., and McVaugh, J. M., "The Dynamics of Rotor-Bearing Systems Using Finite Elements," *Journal of Engineering for Industry ASME*, Vol. 98, pp. 593-600 (1976).

Nelson H.D., "A finite rotating shaft element using Timoshenko beam theory," *Journal of Mechanical Design ASME*, Vol. 102, pp. 793-803 (1980).

Ruhl, R. L., and Booker, J. F., "A Finite Element Model for Distributed Parameter Turbo-rotor System," *Journal of Engineering for Industry ASME*, Vol. 94, pp. 126-132 (1972).

Thomsen, K. K., and Andersen, H., "Experimental Investigation of a Simple Squeeze Film Damper," *Journal of Engineering for Industry ASME*, Vol. 96, pp.427-430 (1974).

Vance, J. M., and Kirton, A. J., "Experimental Measurement of the Dynamic Force Response of a Squeeze-Film Bearing Damper," *Journal of Engineering for Industry ASME*, Vol. 97, pp.1282-1290, (1975).

Wang, Q. Zhao, B. Fu, Y. Kang, X. and Ma, H., "An improved time-varying mesh stiffness model for helical gear pairs considering axial mesh force component," *Mechanical Systems and Signal Processing*, Vol. 106, pp. 413-429, (2018).

Yang, F., Huang, Q., Wang, Y., and Wang, J., "Research on Dynamics of Double-Mesh Helical Gear Set," *Applied Mechanics and Materials*, Vol. 215, pp. 1021-1025 (2012).

Zhang, Y., Wang, Q., Ma, H., Huang, J., and Zhao, C., "Dynamic Analysis of Three-Dimensional Helical Geared Rotor System with Geometric Eccentricity," *Journal of Mechanical Science and Technology KSME*, Vol. 27, pp. 3231-3242 (2013).

具油膜軸承的斜齒輪轉子系統動態特性之分析

陳膺中
中華民國空軍軍官學校 航空機械工程學系

呂文正　崔兆棠
國立成功大學 航空太空工程學系

摘 要

本研究採用有限元方法來分析具油膜軸承的斜齒輪轉子系統的動態特性。該系統包括旋轉軸、斜齒輪對和油膜軸承。旋轉軸模擬為 Timoshenko 樑，其考慮了旋轉軸的旋轉慣性和剪力效應。斜齒輪對假設為兩個剛性轉盤，沿著壓力線以線性彈簧和阻尼來模擬斜齒輪對的接觸。本研究探討了軸承潤滑粘度、軸承徑向間隙、軸承直徑、軸承長度、軸承長度與直徑之比、螺旋角以及旋轉軸的內徑對系統軸向和橫向動態響應的影響。數值結果可作為提供進一步研究帶有油膜軸承的斜齒輪轉子系統的學術研究人員和工業從業人員的參考。